PERGAMON

Deep-Sea Research II 49 (2002) 4051–4067

DEEP-SEA RESEARCH
PART II

www.elsevier.com/locate/dsr2

Low-frequency variability of the exchanged flows through the Strait of Gibraltar during CANIGO

Jesús García Lafuente[a,*], Javier Delgado[a], Juan Miguel Vargas[a], Manuel Vargas[b], Francisco Plaza[a], Tarek Sarhan[b]

[a] *Departamento de Física Aplicada II, Universidad de Málaga, Campus de Teatinos, 29071 Málaga, Spain*
[b] *Instituto Español de Oceanografía, Laboratorio Oceanográfico de Málaga, Fuengirola, Málaga, Spain*

Received 7 April 2000; received in revised form 7 September 2000; accepted 29 October 2000

Abstract

Time series of the exchanged flows through the Strait of Gibraltar at the eastern section have been estimated from current-meter observations taken between October 1995 and May 1998 within the Canary Islands Azores Gibraltar Observations (CANIGO) project. The inflow exhibits a clear annual signal that peaks in late summer simultaneously with a deepening of the interface. The cycle seems to be driven by the seasonal signal of the density contrast between the surface Atlantic water that forms the inflow and the deep Mediterranean water of the outflow. The outflow and the depth of the interface have predominant semiannual signals and a smaller annual one whose phase agrees with that of the density contrast as well. Local wind stress and atmospheric pressure difference between the Atlantic and the Western Mediterranean to less extent have clear semiannual signal, so that the possibility that the semiannual cycle of the outflow and of the depth of the interface are forced by them was analyzed.

The composite Froude number in this section is well below the critical value, suggesting submaximal exchange. Therefore, the conditions in the Alboran basin influence the exchange and some evidence that the size and location of the Western Alboran Gyre contribute to the observed signals, both annual and semiannual, is provided.

1. Introduction

The inverse estuarine circulation of the flows through the Strait of Gibraltar, which is driven by the net evaporative loss of fresh water in the Mediterranean Sea, exhibits marked temporal variability on different time scales, ranging from a few minutes, associated with the short-length internal waves of near Brunt Väisälä frequency (Watson and Robinson, 1990), to inter-annual variabilities, which are not well known.

The average long-term inflow of Atlantic water, Q_1, and outflow of Mediterranean water, Q_2 ($Q_2<0$), must satisfy the conservative law $Q_1+Q_2=E-P$, where E is the evaporation in the Mediterranean and P includes both precipitation and rivers discharge into the sea. Estimates of the exchanged flows using direct current-meter observations give a value of about 0.8 Sv (1 Sv = 10^6 m^3/s^1) for both inflow and outflow (Bryden et al., 1994; Bascheck et al., 2001), a flow smaller than those historically reported. Tidal flows are

*Corresponding author. Tel.: +34-952-13-2721; fax: +34-952-13-2721.
E-mail address: glafuente@ctima.uma.es (J.G. Lafuente).

0967-0645/02/$ - see front matter
PII: S0967-0645(02)00142-X

much greater and produce periodic semidiurnal flow reversals in the layers (Candela et al., 1990; Bryden et al., 1994; García Lafuente et al., 2000). Important sub-inertial variability is known to be forced by atmospheric forcing (Candela et al., 1989) in the frequency band of 0.1–0.3 cycles per day (cpd). Annual or semiannual signals, whose amplitudes are smaller, have been analyzed by Bormans et al. (1986) from the difference in sea level between Ceuta and Gibraltar (see Fig. 1). They estimate an annual signal of 6% (within a factor of 2) in the inflow, based on a clear overestimated mean inflowing velocity of 1.2 m/s, with maximum inflow in spring. Bryden et al. (1994), using current-meter observations, report a larger annual signal in Q_1 (around 15%), with a maximum in late summer, and a much smaller amplitude in the Q_2 (4%), with a maximum outflow in January. The strong asymmetry of these values could be the consequence of the short length of their time series, which did not cover one year. However, the data analyzed in the present work provide similar results, suggesting that they might have physical consistency.

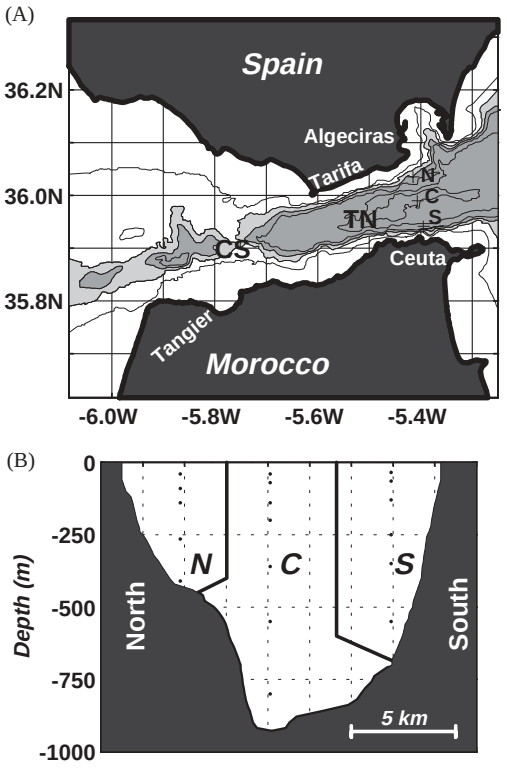

Fig. 1. (A) Map of the Strait of Gibraltar showing some topographic features. Isobaths have not been labeled for clarity. "CS" stands for Camarinal Sill, "TN" stands for Tarifa Narrows. Isobath depths are 100, 200, and 290 m (to illustrate the depth of the sill), 400, 700, and 900 m. Depths > 290 m are in light grey shadow, and those > 400 m in deep grey shadow. Letters N, C and S indicate the position of the mooring lines. (B) Cross section along the mooring array. Dots indicate the current-meter depths. Solid lines divide the overall section into the three subsections used to estimate the flows.

A simple but powerful model for the exchange through the Strait is the two-layer hydraulic control theory. It predicts maximal exchange if the flow is controlled at two sections connected by a subcritical region (Farmer and Armi, 1986). The candidate locations for control are the narrowest section off Tarifa (Tarifa Narrows, TN) and the section of minimum cross-area, also of minimum depth, of Camarinal Sill (CS). At the controls the composite Froude number

$$G^2 = F_1^2 + F_2^2 = \frac{u_1^2}{g'h_1} + \frac{u_2^2}{g'h_2} \tag{1}$$

is critical, $G^2 = 1$. Here $F_i^2 = u_i^2/g'h_i$ is the internal Froude number of layer i, whose velocity and thickness are u_i and h_i, respectively, $g' = g(\rho_2 - \rho_1)/\rho_2$ is the reduced gravity, and ρ_i is the layer density. Bryden and Kinder (1991) applied this theory to the Strait of Gibraltar to estimate the steady exchanged flows using a realistic topography and complying the flows to satisfy conservative laws for salt and mass in the Mediterranean. Their predictions agree within 20% with the observations for the accepted values of $E - P$.

Farmer and Armi (1986) incorporated barotropic signals into the model using a quasi-steady approximation in which the steady solution is verified at each point of the cycle. Helfrich (1995) showed that this approach is only valid for dynamically short straits, a concept related to the parameter $\gamma = (g'h_1)^{1/2}T/L$ that measures the length L of the strait relative to the distance an internal signal will travel during the forcing period T of the barotropic signal. The quasi-steady approximation is only valid for $\gamma \to \infty$, a condition widely fulfilled by low frequency signals but not by

tidal fluctuations (Helfrich, 1995; García Lafuente et al., 2000).

The model can still be applied to a situation of submaximal exchange in which the control at TN is lost. In this case, the interface in the Strait would respond to changes in the Mediterranean since it is now possible for a signal to travel upstream through the Strait into the Atlantic Ocean. Bormans and Garrett (1989) developed these ideas in order to reconcile experimental observations at the eastern entrance of the Strait, which pointed to clear submaximal exchange, and the model predictions. In fact, they used a particular solution of the model, known as marginally submaximal exchange, in which the flow east of the contraction remains subcritical but the flows exchanged are still maximal. This solution can be considered as a limit of the strictly submaximal solution for increasing flows. Whether the exchange is maximal or submaximal is still a matter of controversy. Both types of exchanges have been reported in the literature (see Garrett (1996) for an extensive and interesting review on the subject).

In the case of submaximal exchange, the basins are not isolated from each other and the conditions in the Mediterranean Sea directly affect the flows. The westernmost basin of the sea is usually occupied by a large anticyclonic gyre (see Lanoix (1974) for instance). It exhibits a large time variability (Heburn and La Violette, 1990) that must be taken into account to provide a consistent description of the flow variability if the exchange is submaximal.

This work analyses the annual and semiannual signals in the exchange based on long time series acquired in the frame of the Canary Island Azores Gibraltar Observations (CANIGO) European Union project.

2. Data and methods

2.1. Data-set

From October 1995 to May 1998 a mooring array of recording currentmeters was deployed in the eastern part of the Strait of Gibraltar within CANIGO to help resolve the different time-scales of the exchange. Figs. 1A and B roughly show the position and depth of the instruments. A wide variety of problems have reduced the available information to that summarized in Table 1. For convenience, the entire period of observations has been divided into three sub-periods, which shall be referred to as PP (for "Pilot Phase", spanning from October 1995 to May 1996), P2 (for "Period 2", from July 1996 to July 1997) and IP (for "Intensive Phase", from July 1997 to May 1998). The spatial coverage during PP was good, but not so during P2 when only the North line worked properly. During IP the north line was lost, hence no information from this location is available.

Meteorological data during the same period as the oceanographic observations were collected from the Instituto Meteorológico Nacional (IMN). They include local atmospheric pressure and winds in Tarifa and Ceuta, as well as the average atmospheric pressure over the Gulf of Cádiz and the Western Mediterranean (from daily forecast bulletins published by IMN). Sea-level data also were collected in Algeciras, Tarifa (on the north shore of the Strait) and Ceuta (south shore).

2.2. Transport estimates

Tidal currents can contribute to the mean flow through well-defined correlations between the interface oscillation and the strength of the current (Bryden et al., 1994). Contrary to CS, this mechanism is not important in the eastern section (García Lafuente et al., 2000). Therefore, the slowly varying transport here can be estimated uniquely using the tidal-free velocity measurements. Details of the procedure used to obtain these velocities can be seen in García Lafuente et al. (1998, 2000).

The velocities obtained in this manner have a typical baroclinic structure. The subinertial meteorologically forced fluctuations are not strong enough generally to reverse flows in either layer, so that the surface of along-strait null velocity is well-defined and considered as the interface. The inflow Q_1 and the outflow Q_2 are computed according to

Table 1
Sketch of the temporal and spatial coverage of the current-meter data used to estimate flows

Position	Depth (m)	1995								1996												1997												1998					
		O	N	D	J	F	M	A	M	J	J	A	S	O	N	D	J	F	M	A	M	J	J	A	S	O	N	D	J	F	M	A	M						
North 36º02.4N 5º23.7W	40	■	■	■	■	■	■	■	■		■	■	■	■	■	■	■	■	■	■	■	■	■																	
	90	■	■	■	■	■	■	■	■		■	■	■	■	■	■	■	■	■	■	■	■	■																	
	140	■	■	■	■	■	■	■	■		■	■	■	■	■	■	■	■	■	■	■	■	■																	
	265	■	■	■	■	■	■	■	■		■	■	■	■	■	■	■	■	■	■	■	■	■																	
	430	■	■	■	■	■	■	■	■		■	■	■	■	■	■	■	■	■	■	■	■	■																	
Center 35º59.7N 5º23.2W	40	■	■	■	■	■	■	■	■															■	■	■	■	■	■	■	■	■	■	■	■	■	■	■	■
	70	■	■	■	■	■	■	■	■															■	■	■	■	■	■	■	■	■	■	■	■	■	■	■	■
	140	■	■	■	■	■	■	■	■															■	■	■	■	■	■	■	■	■	■	■	■	■	■	■	■
	200	■	■	■	■	■	■	■	■															■	■	■	■	■	■	■	■	■	■	■	■	■	■	■	■
	360	■	■	■	■	■	■	■	■															■	■	■	■												
	550	■	■	■	■	■	■	■	■															■	■			■	■	■	■	■	■	■	■	■	■		
	800	■	■	■	■	■	■	■	■															■				■	■	■	■	■	■	■	■	■	■	■	
South 35º51.7N 5º21.5W	35																							■	■	■	■	■	■	■	■	■	■					■	■
	65																							■	■													■	■
	130																							■	■	■	■	■	■	■	■	■	■	■	■	■	■	■	■
	250	■	■	■	■	■	■	■	■															■	■	■	■	■	■	■	■	■	■	■	■	■	■	■	■
	350	■	■	■	■	■	■	■	■															■	■	■	■	■	■	■	■	■	■	■	■	■	■	■	■
	550																							■	■	■	■	■	■	■	■	■	■	■	■	■	■	■	■

PILOT PHASE (1995 O N D J F M A M J)
PERIOD 2 (1996 J A S O N D J F M A M J J)
INTENSIVE PHASE (1997 J A S O N D J F M A M and 1998 J F M A M)

Gray squares mean instrument failures. The three sub-periods mentioned in the text are also indicated.

$$Q_1(t) = \int_y \int_{\eta_2(y,t)}^{0} u(y,z,t)\,\mathrm{d}z\,\mathrm{d}y, \tag{2}$$

$$Q_2(t) = \int_y \int_{\mathrm{bottom}(y)}^{\eta_2(y,t)} u(y,z,t)\,\mathrm{d}z\,\mathrm{d}y, \tag{3}$$

where $\eta_2(y,t)$ is the depth of the interface at instant t, and $u(y,z,t)$ is the along-strait velocity, which has been filtered with a Gaussian-like filter of 0.25 cpd cut-off frequency. The Cartesian reference system has been rotated $+17^\circ$ in order to have the x-axis oriented along strait. The y-axis points to the north shore and the z-axis is positive upwards. The depth of the interface has been determined by linear interpolation between the two depths at which $u(y,z,t)$ changes sign. The integrals above have been replaced by summations over the three boxes sketched in Figure 1B. Each vertical box allows for estimations of partial flows through them. Low-frequency velocities at the same depths in the center and south moorings taken during IP are highly correlated ($r^2 > 0.93$). This fact has been used to infer inflowing velocities at the south mooring from observations at the central one in order to supplement the lack of information present during PP. The velocities measured by each mooring line and those extrapolated in the south during PP are considered to be representative of each subsection. They have been interpolated/extrapolated to obtain a velocity every 10 m and multiplied by the cross area associated with the 10-m thick bin to obtain the flows. Details of the computation can be seen in García Lafuente et al. (2000).

Table 1 indicates that such computation is not feasible during P2 and IP. In these cases linear extrapolations to obtain total flows from partial flows have been made.

2.2.1. Regression model

The following very simple model has been used:

$$y = y_0 + h(x - \bar{x}), \tag{4}$$

where y is the output, x and $\bar{x}$ are the input and its mean, respectively, and y_0 and h are the model parameters. During P2, the outputs were the total flows, Q_1 and Q_2, and η_{2C} (the depth of the interface at the center line, which will be considered the reference depth of the interface at the eastern section throughout this paper) and the

inputs Q_{1N}, Q_{2N} and η_{2N} (partial inflow and outflow through the northern subsection and depth of the interface at this point). During IP the inputs were Q_{1C} and Q_{2C} and the outputs Q_{1N} and Q_{2N}, which added up to Q_{1C} and Q_{1S} (Q_{2C} and Q_{2S}) giving the total inflow (outflow). In all cases the model parameters have been estimated with the data taken during PP, when the spatial coverage was good. Table 2 shows the parameters with their errors at a 95% significance level. The extrapolations for estimating Q_1 and η_{2C} during P2 had good statistical confidence and a high correlation coefficient whereas Q_2 was not so well determined. The poorest correlation coefficient was obtained when inferring Q_{2N} from Q_{2C} during IP. Nevertheless the contribution of the former to the total outflow is very small, so that the final estimation of Q_2 is not overly affected by this fact.

The model of Eq. (4) could have been extended to a multiple regression model including more input variables such as cross-strait sea-level slopes, wind stress, atmospheric pressure differences, etc. This would have improved the value of r^2 in all cases but reduced the statistical confidence of the regression. Moreover, such a model introduces artificial correlations between the input variables and the output, which does not seem advisable if one is looking for independent correlations between external agents and the flows or the depth of the interface. This is the reason why the simple model of Eq. (4) was used.

2.2.2. Means

The procedure to obtain flows through Eqs. (2) and (3), along with the instrumental errors and the commented extrapolations, make the accepted flows during the whole period somewhat uncertain. Merging the subseries can produce jumps in the junctions. To analyze very low-frequency signals (annual and semiannual cycles) it has been assumed that the mean value from October 1995 to May 1996 (the whole PP), from October 1996 to May 1997 (a fraction of P2) and from October 1997 to May 1998 (a fraction of IP) should be approximately the same. Other time series such as atmospheric pressure or sea level did not exhibit trends, a fact that supports this assumption. A correction of Q_1 and Q_2 during periods P2 and IP has been made to bring together the means. The near one-year length of these series prevents the introduction of spurious signals as would be the case if PP were corrected, since a correction of the mean in a six-month time series would introduce an artificial annual signal.

The final time series of Q_1, Q_2 and η_{2C} are shown in Fig. 2. Their means and standard deviations are 0.97 ± 0.14 Sv, -0.84 ± 0.09 Sv and -128 ± 12 m, respectively, which are only indicative due to the way in which they have been obtained. More elaborated computations, based on an inverse model that includes the most important tidal constituents applied to 1-year long

Table 2
Adjustment parameters of the model of Eq. (4)

Output	y_0	h	r^2	F
Q_1 (P2)	0.35 ± 0.03	3.89 ± 0.02	0.83	1681
Q_2 (P2)	-0.63 ± 0.03	2.80 ± 0.25	0.58	486
η_{2C} (P2)	-67.1 ± 4.0	0.49 ± 0.03	0.73	924
Q_{1N} (IP)	-0.013 ± 0.01	0.434 ± 0.023	0.75	1059
Q_{2N} (IP)	0.036 ± 0.027	0.191 ± 0.038	0.22	99

Last two columns give the regression coefficient and the statistical F of the model. The intervals of confidence are at 95% significance level. The different outputs are explained in the text.

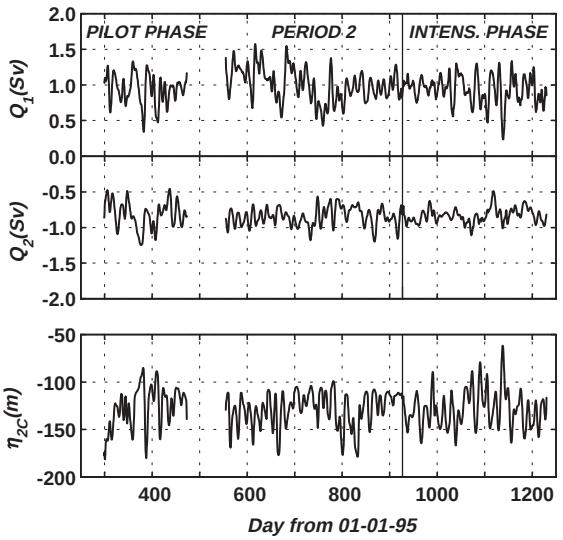

Fig. 2. Time series of the flows estimated from the data set (top panel) and depth of the interface at the Centre mooring line (bottom panel).

data set, suggests around a 10% drop in mean flows (Bascheck et al., 2001). The figures above tally with these results within a standard deviation. Nevertheless, the main objective of this work is to investigate annual and semiannual signals, which probably have not been masked by data processing.

3. Low-frequency signals

Fig. 2 shows that most of the variance resides in the high (but still subinertial) frequency band. To remove high-frequency variability, blocks 15-day long that overlap 7.5 days have been averaged over and the resulting series smoothed again with a filter of weights 0.25, 0.5, and 0.25. The standard deviation within each block is taken as the error of the estimate. These new series, which are plotted in Fig. 3, have been analyzed to investigate annual and semiannual cycles. The existence of signals of frequencies $f_a = 1$ cycle per year $= 1.99 \times 10^{-7}$ rad/s and $f_s = 2f_a = 3.98 \times 10^{-7}$ rad/s have been assumed and the model

$$y = y_0 + B(t - t_m) + A_a \cos(f_a t - \varphi_a) + A_s \cos(f_s t - \varphi_s) + \varepsilon \quad (5)$$

has been adjusted to the data. Here A_a and A_s are the amplitudes of the annual and semiannual cycles, φ_a and φ_s their phases (which refer to the beginning of 1995, that is, to the beginning of the year), and ε is the unexplained residue of zero mean. The parameter B is included to allow for trends (but in all cases it is not statistically different from zero, as can be expected after making the mean adjustment mentioned above), t_m is the time of the midpoint of the series, and y_0 is a parameter that would be identified with the mean value of y. Table 3 shows the value of the different parameters and their errors at 95% confidence level for Q_1, Q_2 and η_{2C}. The most noticeable feature is the existence of a significant annual cycle for Q_1, this being less significant for Q_2 and Q_{2C}, both of which have semiannual dominance. The ratio A_s/A_a for the latter variables is around 2 and their phases suggest that they are correlated (note that $\varphi_s = 174^\circ$ for Q_2 becomes $\varphi_s = 354^\circ$ for $|Q_2|$, which is within the error of φ_s for η_{2C}).

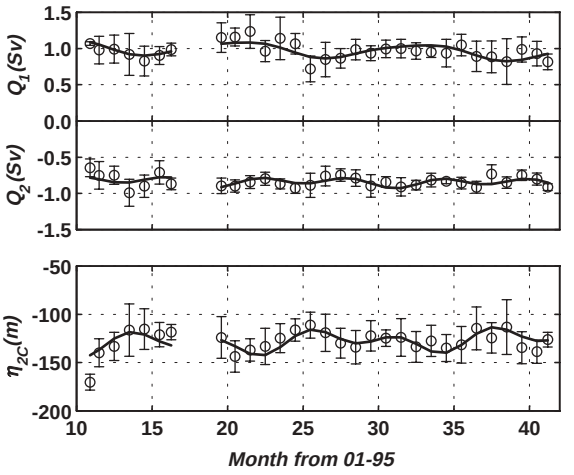

Fig. 3. Fifteen-day averaged time series of the flows and the interface depth at the Center mooring line (dots, upper panel and lower panels, respectively) and standard deviation for these means (bars). Only one mean per month has been displayed for clarity. The solid line is the fitted curve of the model of Eq. (5).

3.1. The annual cycle

The annual signal in Q_1 can be a consequence of a signal in the inflowing velocity, in the cross-area, or in both. In a two-layer sea, $Q_1(t) = U_1(t)A_1(t)$ where $U_1(t)$ is the (uniform) time-dependent inflowing velocity and $A_1(t)$ is the time-dependent cross-area of the layer. It changes mainly due to interface oscillations, so that $U_1(t) = Q_1(t)/(\eta_{2C}(t)W)$, where $W = 14500$ m is the width of the Strait. Table 3 shows the result of applying Eq. (5) to this velocity. The annual cycle of U_1 and η_{2C} (and, hence, of A_1) are $\sim 7.2\%$ and $\sim 3.5\%$ of their mean values, respectively. They will contribute in the same proportion to the annual cycle of the inflow, that is, velocity fluctuations contribute twice as much as interface fluctuations. The rectified transport arising from the positive correlation between interface and velocity fluctuations is evaluated in $<0.1\%$ of the mean inflow and, hence, can be neglected.

Bryden et al. (1994) provide the only estimates of annual signals in the exchanged flows based on

Table 3
Estimated parameters of the model of Eq. (5) for the different variables given in the first column

	Y_0	ΔY_0	A_a	ΔA_a	φ_a	$\Delta\varphi_a$	A_s	ΔA_s	φ_s	$\Delta\varphi_s$	r^2	rmse	χ^2
Q_1 (Sv)	0.99	0.06	0.101	0.038	225	21	0.015	0.035	244	130	0.41	0.095	62
Q_2 (Sv)	−0.84	0.04	0.028	0.025	21	51	0.057	0.021	174	20	0.28	0.069	70
Q_0 (Sv)	0.14	0.07	0.077	0.044	234	33	0.064	0.035	187	31	0.32	0.114	48
η_{2C} (m)	−128.72	5.15	4.557	3.269	61	42	8.020	2.897	14	21	0.37	8.684	80
$\Delta\xi_T$ (cm)	10.15	1.69	0.676	0.922	101	82	1.939	1.101	312	33	0.28	2.856	344
Δp_a (mb)	1.00	1.06	0.338	0.702	216	118	0.727	0.572	281	46	0.09	1.787	146
U_w (m/s)	0.49	0.68	0.098	0.439	209	251	1.206	0.439	311	21	0.35	1.142	169
U_1 (m/s)	0.53	0.03	0.039	0.023	216	33	0.024	0.017	356	39	0.27	0.057	155
U_2 (m/s)	−0.13	0.01	0.005	0.004	26	43	0.008	0.003	171	23	0.27	0.010	69
$\Delta\rho$ (kg/m^3)	2.42		0.29		238		0.03		289				

Y_0 and ΔY_0 are the mean value and its 95% confidence interval, A_j, φ_j, ΔA_j, and $\Delta\varphi_j$ are amplitude and phase and their confidence intervals for annual ($j = a$) and semi-annual ($j = s$) signals, respectively. Last three columns give statistical estimators of the fitting; r^2 is the squared regression coefficient, rmse is the root mean square error and χ^2 is the chi-square value of the fitting. The critical value of χ^2 at the 95% significance level is 135. Third row is the absolute value of the outflow, that is, $-Q_2$. $\Delta\xi_T$ is the across strait sea level difference computed as sea level in the south shore (Ceuta, see Fig. 1) minus sea level in the north shore (Algeciras). Δp_a is the atmospheric pressure difference between the Gulf of Cadiz and the Western Mediterranean Sea. U_w is the along-strait component of wind observed in Ceuta. U_1 and U_2 are the cross-strait averaged velocity of the inflow and outflow, respectively, and $|U_2|$ is the absolute value of the latter. Finally, $\Delta\rho$ is the density difference between Mediterranean and Atlantic water. See text for more details.

experimental observations. Their data set spanned over less than one year so that the cycle is not well-defined. They report annual signals of 0.12 Sv at 264° for Q_1, 0.03 Sv at 23° for $|Q_2|$ and 18 m at 41° for η_{2C} in CS. The concordance between the amplitude and phase of Q_1, and between the amplitude of $|\eta_2|$ and the phase of η_{2C} is good.

The last row of Table 3 shows the annual and semiannual cycles of the difference of densities $\Delta\rho$ between Atlantic surface water and Mediterranean deep water reported by Bormans et al. (1986) and determined from a long historical data set of salinity and temperature in the Strait of Gibraltar and its surroundings. The clear annual signal in $\Delta\rho$ and the good agreement with the phase of Q_1 suggest that the inflow annual cycle is caused by the seasonal signal in the density difference, which does not exhibit a semiannual signal either. The question of why the annual signal in $\Delta\rho$ would not induce a comparable signal in the outflow, which remains rather insensitive, is discussed in Section 5.

3.2. The semiannual cycle

This is the prevailing signal in Q_2 and η_{2C}. Their phases suggest good correlation between them: the greater the outflowing section (that is, the higher the interface) the greater $|Q_2|$. The interface oscillation is, however, unable to account for the observed amplitude of the outflow. Its amplitude only changes the outflowing section by 2.5%, which is less than the 7% variation estimated in the outflow. An additional signal in the outflowing velocity U_2 is needed in order to explain the estimated semiannual fluctuation. Similar computations as those carried out previously provide the amplitude and phase presented in Table 3. The semiannual signal is clear and it has the necessary value to explain the remaining percentage.

One possible force to drive the semiannual cycles could be wind-stress, which also exhibits quite a clear semiannual signal (see Table 3). Wind stress correlates positively with the atmospheric pressure differences between the Atlantic (Gulf of Cadiz) and western Mediterranean basins (correlation coefficient of 0.75), which also has a dominant semiannual cycle. The phases of the semiannual cycles of $|Q_2|$ and η_{2C} lag by 43° and 63° (21 and 31 days), respectively, to wind stress, which does not disagree with a cause–effect relationship. The lagged correlation between wind stress and the interface depth shows a peak of 0.6 for a lag of this magnitude. Some speculative arguments put for-

ward to explain the links between wind stress and Q_2 and η_{2C} are also discussed in Section 5.

3.3. Net barotropic signals and the Mediterranean sea level cycles

3.3.1. Annual signals

Inflow and outflow annual signals combine to produce a seasonal signal in the net barotropic flow that peaks in late August. The simplest model in which this signal, Q_{0a}, is balanced within the Mediterranean Sea is

$$Q_{0a} = \mathrm{d}V_{\mathrm{MED}}/\mathrm{d}t \tag{6}$$

(V_{MED} being the volume of the Mediterranean), which ignores the seasonal cycle of $(E-P)$. The equation is readily solved using the Q_0 values shown in Table 3 to give an annual signal of 15 ± 9 cm, with a maximum value in November. Larnicol et al. (1995) provide evidence of a seasonal cycle of the Mediterranean mean sea level of around 10 cm using TOPEX/POSEIDON altimetry data from October 1992 to September 1994. Ayoub et al. (1998) also report a similar signal of 8 cm of amplitude, with a maximum value in October, using ERS-1 and TOPEX/POSEIDON altimetry data from 1993. This annual signal is quite evident in longer time series of altimetry data (P.Y. LeTraon, personal communication). Tsimplis and Woodworth (1994), from coastal tide gauge records, show an annual signal (the Sa tidal constituent) in the Mediterranean sea level that matches well the phase of these altimetry signals but with a smaller amplitude (around 5 cm). The disagreement of amplitudes can be accounted for by the fact that the altimetry signal comes mainly from the open sea while tide gauge data are coastal observations. Part of this signal is due to temperature and salinity steric effects that are given by (Patullo et al., 1955)

$$\xi_T = g^{-1}\int_{p_a}^{p_0} \alpha\rho^{-1}\Delta T\,\mathrm{d}p, \tag{7}$$

$$\xi_S = -g^{-1}\int_{p_a}^{p_0} \beta\rho^{-1}\Delta S\,\mathrm{d}p, \tag{8}$$

where ξ_T (ξ_S) is the sea-level steric anomaly due to temperature (salinity) difference ΔT (ΔS) with respect to the mean at a given depth. Integrals extend from the surface (p_0) to depth p_a, where the seasonal signal does not reach, and α (β) is the coefficient of thermal (haline) expansion of sea water. The MEDATLAS data set (MEDATLAS Consortium, 1997) contains monthly temperature values at fixed depths, which have been optimally interpolated from a large set of in-situ observations covering the whole Mediterranean Sea. It also contains seasonally averaged salinity values. With these data and Eqs. (7) and (8), the steric anomalies at grid points of a roughly regular grid covering the Mediterranean Sea have been estimated. The depth of reference was taken at $p_a = 300$ db. The results for the steric thermal and haline anomalies are presented in Figs. 4A and B, respectively. The solid lines are the annual cycles that best fit to each of them and would be representative of the seasonal cycle of the steric sea level anomaly of the Mediterranean Sea. They have 5.5 ± 0.4 cm of amplitude and $253\pm12^\circ$ of phase (12 September) for the thermal contribution

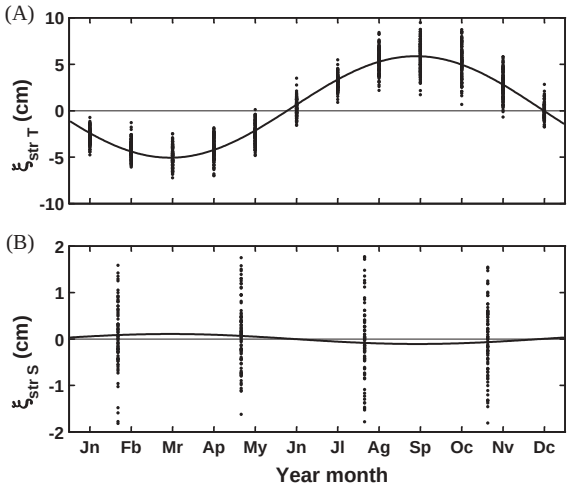

Fig. 4. (A) Thermal steric anomaly of the Mediterranean Sea level calculated from MEDATLAS data base using 300 db as reference. Dots are the monthly anomalies at 133 different sites distributed homogeneously over the Mediterranean Sea. The solid line is the sine least-squares fitted curve to the local anomalies. (B). Haline steric anomaly determined from seasonal values and using the same depth as before. The solid fitted line is not statistically different from zero indicating a null contribution of the haline effect to the total steric anomaly.

and are not significantly different from zero for the haline contribution (0.11 ± 0.24 cm).

When this anomaly is subtracted from the sea level cycle mentioned by Larnicol et al. (1995) or reported by Ayoub et al. (1998) the result is far from the 15 cm of amplitude implied by the Q_0 signal found in this study. The correct mass balance cannot ignore the climatological $(E-P)$ forcing, and Eq. (6) should be re-writen as

$$Q_{0a} - (E-P)_a = \frac{dV_{MED}}{dt} = A_{MED}\frac{d\xi_m}{dt}, \quad (9)$$

where $(E-P)_a$ is the annual signal in the net evaporation, $A_{MED} = 2.5 \times 10^{12}$ m^2 is the area of the Mediterranean Sea, and ξ_m the contribution due to an effective mass variation within the sea. Obviously, $\xi_m = \xi_{obs} - \xi_{str}$, where ξ_{obs} is the observed sea-level signal and ξ_{str} is the steric contribution. With the values provided by Ayoub et al. (1998) and after correcting for the steric anomaly estimated above, the RHS of Eq. (9) takes a value of around 0.02 Sv at 230°, which in turns gives 0.06 Sv at 237° for $(E-P)_a$ using the Q_0 seasonal cycle shown in Table 3. The seasonal net evaporative cycle is difficult to evaluate, in part because of its interannual variability. Evaporation is maximum during late autumn, but the peak of $(E-P)$ is probably shifted towards summer, the dry season, due to the contribution of the precipitation. Carter (1956) suggests a cycle in the Mediterranean of around 6 cm/month (0.06 Sv) that peaks in August (215°). Bormans et al. (1986) consider the values from the World Survey of Climatology (Wallen, 1970) to obtain a seasonal signal of 7.1 cm/month (0.07 Sv) at 181°. The agreement with the values computed from Eq. (9) is satisfactory, particularly regarding amplitudes. The phases will surely agree within the confidence intervals, but it is not possible to provide figures for them due to the lack of information regarding their values for $(E-P)_a$ and ξ_{obs}.

3.3.2. Semiannual signals

The semiannual signal of Q_2 is chiefly responsible for the semiannual cycle of Q_0 indicated in Table 3. The mass balance of Eq. (6), which assumes the absence of a semiannual net evaporative cycle, would induce a sea-level signal in the Mediterranean Sea of 6.4 ± 3.5 cm at $277 \pm 31°$. Ayoub et al. (1998) report a semiannual signal of 4 cm of amplitude in the Eastern Mediterranean Basin that is negligible in the Western Basin. It is equivalent to a signal slightly <3 cm for the whole Mediterranean. However, they do not mention any phase for this signal.

Tsimplis and Woodworth (1994) also give values for the semiannual (Ssa) tidal constituent in the Mediterranean based on tide gauge data (in spite of the fact that they use this tidal nomenclature, they show that the gravitational part is small not only in Ssa but also in the above-mentioned Sa constituent, and that they mainly stem from meteorological, oceanographic and hydrological—river runoff—forcing). This signal has noticeable regional variability but, excluding the Aegean Sea and the far Eastern areas of the Mediterranean, the phases of most of the remaining coastal sea level stations are between -2 and -1 months with reference to the first day of the year (240°–300° in our nomenclature) and the amplitudes range from 1 to 5 cm (3 cm could be a "typical" value). This amplitude roughly coincides with the amplitude determined from altimetry data and both reside in the lower part of the error interval of the estimate from Q_0 cycle shown in Table 3. However, the estimates from coastal tide gauges come from non-simultaneous time series. Taking into account the nature of the semiannual forcing, the regional variability reported by Tsimplis and Woodworth (1994) also could be indicative of interannual variability of the Mediterranean surface circulation, and if this were so their results would not be suitable for comparison with the estimate presented in this study.

The right mass balance for this signal should include climatological forcing as well (Eq. (9)). The semiannual cycle of $(E-P)$, if real, is even more unknown than the annual one. Bormans et al. (1986) mention a signal of 2.5 cm/month (0.024 Sv) at 46°, which gives 0.084 Sv at 197° for the LHS term of equation ecuacion 9. This, in turns, would increase the amplitude of the sea-level signal up to 8.4 cm, the phase being hardly modified (287°). The new amplitude would

disagree even more with the "direct observations" of sea level.

4. Hydraulic control model versus observations

4.1. Some theoretical considerations

One striking result that can be seen in Table 3 is that Q_1 and Q_2 cycles are not coupled, that the cycles of η_{2C} are linked to Q_2 rather than to Q_1, and that the cycles of the net barotropic flow arise as a consequence of this uncoupling. An attempt has been made to interpret these observations in the frame of the hydraulically controlled exchange commented in Section 1.

The maximal exchange situation requires the existence of two control sections, one in Camarinal Sill (CS) and the other in Tarifa Narrows (TN) (see sketch in Fig. 5). Basically, the first one would control the outflow (G_S^2 in Eq. (1) reaches the critical value 1 mainly due to the contribution of F_{2S}^2), while the second one would control the inflow (F_{1N}^2 is the term that brings G_N^2 to critical).

It is easy to show that the above-mentioned results, are not compatible with this maximal exchange situation. For instance: one possibility for flow variations is that g' changes due to seasonal fluctuations in the inflow density. Under maximal exchange, the flows are proportional to $g'^{1/2}$ and both Q_1 and Q_2 must fluctuate in phase. On the other hand, if g' remains constant, any fluctuation of, say, Q_1 must be accomplished by an increment in the inflowing velocity and a deepening of the interface at TN in order to maintain the critical flow there. This perturbation of the interface in TN is capable to progressing freely through the subcritical region west of TN and to reach CS, sinking the interface here. The outflowing velocity must decrease (in modulus) in order to maintain the critical condition in CS so that $|Q_2|$ diminishes. Therefore, an increase of Q_1 produces a decrease of $|Q_2|$ and a deepening of the interface, all variables fluctuating in phase, and both flows contribute approximately by the same amount ($Q_0/2$) to the net barotropic signal. As this does not match the observations made in this work, the maximal exchange state must be rejected.

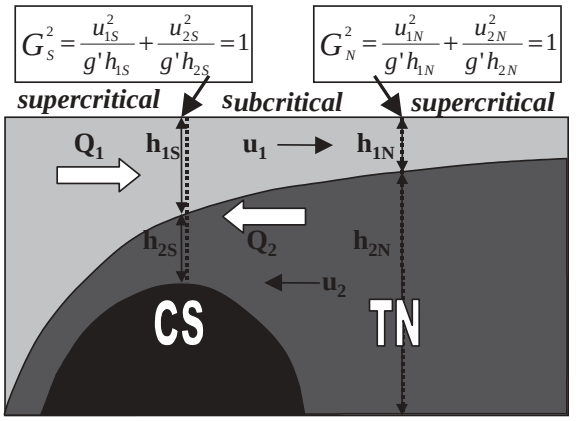

Fig. 5. Sketch of the two-layer model in the case of maximal exchange showing the supercritical and subcritical regions and the control sections.

The outflow is likely to be hydraulically controlled in CS, since water of the same density as the outflow is found at a greater depth in the Atlantic Ocean. Therefore, that the maximal exchange is not achieved should be due to the fact that the TN control section is not present.

4.2. A simple unidimensional model

Under these circumstances it is possible to use the unidimensional model proposed by Bormans and Garrett (1989), who used triangular cross sections to represent the actual topography of the Strait. Their model can take into account the effects of bottom and interfacial friction, although in this work the simpler frictionless model has been used. Rotation effects are not considered, so that the interface has no cross strait structure and its depth can be identified with the η_{2C} estimates given here. They obtain a differential equation with a single unknown ($\eta_2(x)$, see Eq. (4.10) of their work), which has the following form:

$$\frac{\partial}{\partial x}\left[\frac{Q_1^2}{2A_1(x)} - \frac{Q_2^2}{2A_2(x)} - g'\eta_2(x)\right] = 0. \tag{10}$$

This equation can be integrated with the condition of critical flow at CS, which can be written for

triangular geometry as

$$\frac{Q_1^2}{g' A_{1S}^3} + \frac{Q_2^2}{g' A_{2S}^3} = \frac{h_{1S} + h_{2S}}{W_S h_{2S}}, \tag{11}$$

where subscripts 1 and 2 refer to the upper and lower layer, respectively, A and W stand for cross areas and width of the Strait at the surface, respectively, which depend on the position, subscript S is for Sill, and h_1 and h_2 are the thickness of the upper layer and the distance from the interface depth to the sea floor at the axis of the Strait, respectively. Flows Q_1 and $|Q_2|$ may differ so that the model allows for barotropic fluctuations $Q_0 = Q_1 + Q_2$.

Given a barotropic fluctuation Q_0, the model can be integrated if (I) the value of one of the exchanged flows is provided (the other being automatically determined) or (II) the existence of TN control section is assumed, in which case the exchanged flows are determined by the geometry of the Strait and are outputs of the model. Needless to say, they are the maximum allowable flows (maximal exchange). Under this second assumption, one still obtains the two expected solutions, one corresponding to strictly maximal exchange with supercritical flow east of TN, the other corresponding to marginally submaximal exchange with subcritical flow east of TN but with the same exchanged flows. The three possibilities are presented in Fig. 6. Obviously, the Eqs. (10) and (11) have no solution if, in case I, one provides a flow greater than the one obtained in the second situation.

Fig. 7A shows that for maximal or marginally submaximal exchange a positive (negative) barotropic fluctuation Q_0 sinks (raises) $\eta_{2,C}$, the response being greater in the second situation. In these cases, as mentioned above, a barotropic fluctuation of amplitude Q_0 is achieved very approximately by a simultaneously linked fluctuation of amplitude $Q_0/2$ in both Q_1 and Q_2. On the contrary, Fig. 7B shows that under submaximal conditions Q_1 can fluctuate independently of $|Q_2|$ and $\eta_{2,C}$ (thin line). However, the fluctuations of these two variables are still linked to each other (thick line) as a consequence of the outflow being controlled at CS. Thus, a barotropic fluctuation of

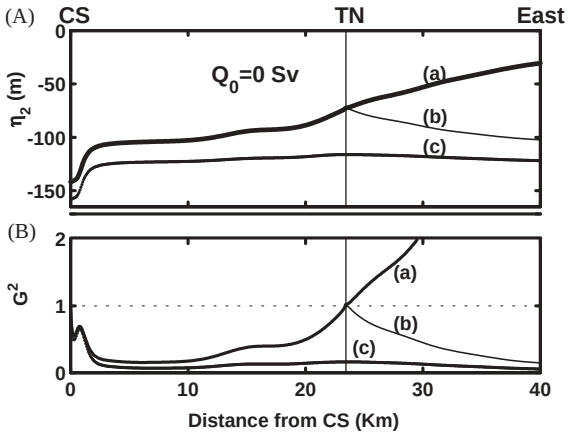

Fig. 6. (A) Solution of Eqs. (10) and (11) for the interface height between CS and the eastern section for the maximal (a), marginally submaximal (b) and submaximal (c) exchanges and zero net barotropic transport. (B) Composite Froude number G^2 for these three situations.

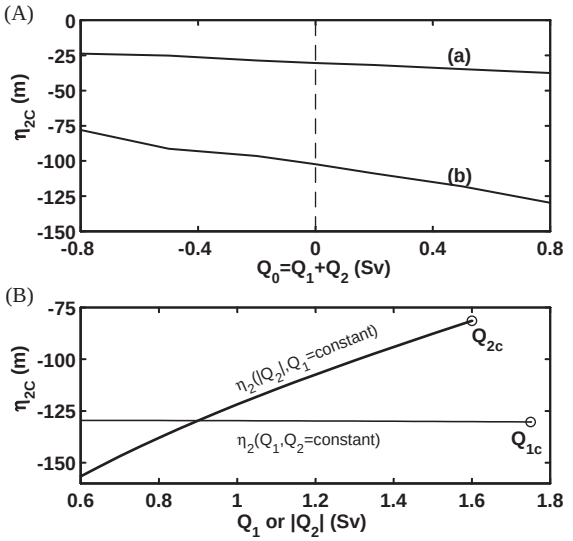

Fig. 7. (A) Interface height at the eastern section as a function of the net barotropic transport for the maximal (a) and marginally submaximal (b) exchanges. (B) Interface height fluctuations as a function of the net barotropic transport for submaximal exchange if the inflow remains constant (thick line) or if the outflow remains constant (thin line). The barotropic fluctuation is achieved by outflow variations in the first case and by inflow variations in the second one, which in these circumstances are not coupled. Dots labeled Q_{2C} and Q_{1C} indicate that for these values of the net barotropic flow, the exchange has been brought to maximal.

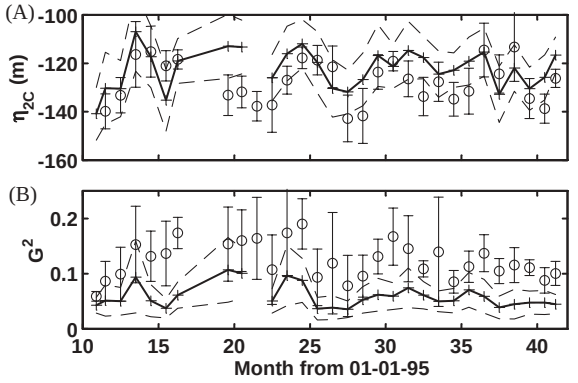

Fig. 8. (A) Prediction of the interface height at the eastern section given by Eqs. (10) and (11) (thick line) using the values of Q_1 and Q_2 of Fig. 3. The 95% confidence interval is indicated by the thin dashed line. Dots are the observations with their error bars, as in Fig. 3. (B) Same as in (A) for the composite Froude number G^2 at the eastern section.

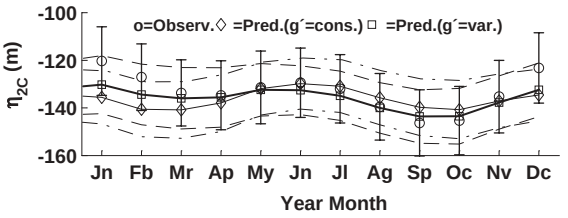

Fig. 9. Predictions of the interface height at the eastern section given by Eqs. (10) and (11) using monthly values during the entire period of observations and taken g' as constant (thin line, diamond symbol) and considering the annual cycle of g' (thick line, rectangle symbol). Dashed lines are the 95% confidence interval for the predictions. Dots and error bars are the monthly averaged observations.

amplitude Q_0 can be achieved by independent fluctuations of Q_1, or of Q_2, or both. This result agrees with the authors' observations. Fig. 8A shows that the prediction of $\eta_{2,C}$ given by the model using the values of Q_1 and Q_2 shown in Fig. 3 as inputs compares well with the estimated interface depth from the data (correlation coefficient of 0.57). Fig. 8B shows that the composite Froude number is well below the critical value, strongly suggesting submaximal exchange.

The variations of g' have not been considered in the former discussion. The model has been run with a constant density contrast. To assess the influence of g' cycle on the predictions it has been incorporated into the model and compared with the observations. The comparison has been made on the basis of monthly means and standard deviations from the data. That is, all January observations have been averaged together to give a representative value for January, the same being done for the rest of the months of the year. The results are presented in Fig. 9 along with the predictions of the model with and without g' cycle. The correlation coefficient rises up to of 0.93 in the first case (g' cycle). Probably this very high value is somewhat coincidental, but it is also indicative of the influence of the seasonal density signal on the exchanged flows.

5. Discussion

Let Table 3 be examined in greater detail. The annual cycle seems forced by the seasonal signal of $\Delta\rho$ (that is, by g'). Variations in g' do not imply necessarily a phase-locked barotropic fluctuation Q_0. In fact, Fig. 10B shows how under maximal (or marginally submaximal) conditions the inflow and outflow change as $\sqrt{\Delta\rho}$ while the net barotropic flow is null. In these circumstances, the interface at the eastern end of the Strait remains practically motionless (Fig. 10A). Since the marginally submaximal situation is the physical limit of increasingly submaximal exchange, one would think that the latter should respond similarly to g' variations, that is, without appreciable barotropic signal and no interface motions. This is not the case in Table 3. The annual signal of Q_1 is much greater than that of Q_2, and produces a clear signal in Q_0. In addition the interface oscillates in such a manner that it is deeper when Q_1 peaks and vice versa. Since the annual cycle of g' does not imply the existence of a corresponding annual cycle in Q_{2C}, the possibility of this cycle being associated to interface oscillations in the Western Alboran Basin has been considered. Under submaximal conditions, the position of this interface represents an effective driving force for the flows, which is independent of the direct influence that g' exert on the exchange via Eqs. (10) and (11).

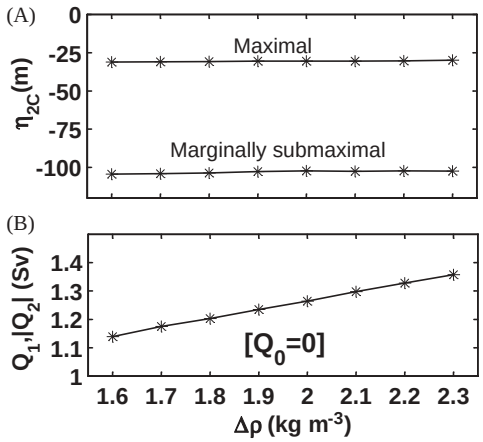

Fig. 10. (A) Depth of the interface at the eastern section given by Eqs. (10) and (11) as a function of the density contrast between inflow and outflow for maximal and marginally submaximal exchanges and zero net barotropic transport. (B) Inflow and outflow dependences on the density contrast for maximal (and marginally submaximal) exchange with zero net barotropic transport.

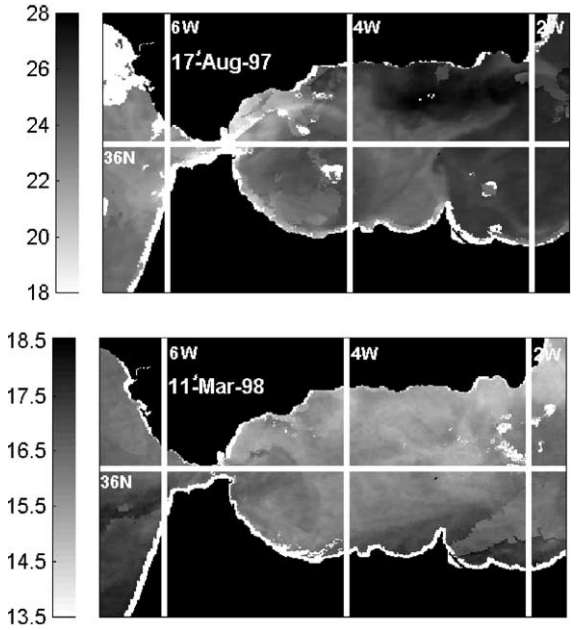

Fig. 11. Sea-surface temperature of the Strait of Gibraltar and Alboran Sea taken by the AVHRR sensor on board the NOAA-14 satellite on August 17th, 1997 and March 11th, 1998. Dark (light) tones correspond to warm (cold) water.

Thus, one can speculate with an interface in the Western Alboran Basin that, on average, it is deeper in summer than in winter. Its actual position will depend on the size and depth of the Western Alboran Gyre (WAG). Numerical simulations indicate that the gyre dimensions are very closely related to the density gradient (Pinardi et al., 1997), so that the greatest gyres will be found in summer. Gleizon (1994) found a clear tendency of the gyre to be more stable when the internal radius of deformation increases. He also points out that greater inflows help develop larger gyres in shorter periods. Plaza et al. (1999) analyze sea-surface temperature (SST) infrared images from 1997 and 1998 and detect a clear tendency for the WAG to be stable and well-developed during summer and early autumn (see Fig. 11). The same result is reported by Ayoub et al. (1998) after analyzing ERS-1 and TOPEX/POSEIDON altimetry data from the Mediterranean.

Csanady (1979) analyzes the size and vertical shape of an ideal circular anticyclonic eddy formed by water of density ρ_1 above a motionless layer of density ρ_2, which is in geostrophic equilibrium and whose potential vorticity is conserved from an initial state. He shows that the depth of the interface of the gyre, $h(r)$, at a distance r from the center is given by

$$h(r) = h_0\left(1 - \frac{I_0(r/R_i)}{I_0(r_G/R_i)}\right), \tag{12}$$

where I_0 is the modified Bessel function of order 0, r_G is the radius of the gyre, that is, the distance at which $h(r)$ vanishes, and $R_i = f^{-1}\sqrt{g'h_0}$ is the internal radius of deformation. Depth h_0 is the thickness of the layer of density ρ_1 in a place where its relative vorticity vanishes, which should be considered the source site for the waters in the gyre. In this case it could be a place west of the Strait in the Gulf of Cadiz, far enough to have negligible velocity. Eq. (12) assumes the conservation of vorticity while this water flows through the Strait to finally form the WAG. The depth of this idealized gyre at its center is

$$h(0) = h_0\left(1 - \frac{1}{I_0(r_G/R_i)}\right) \tag{13}$$

which is a monotonic function of r_G/R_i. The greater this parameter, the deeper the interface.

During summer, both r_G and R_i increase. According with the annual cycle of $\Delta\rho$ in Table 3, the relative variation of R_i is $<6\%$. The seasonal variation of r_G is complicated to determine but appears to be clearly above this figure. If so, r_G/R_i increases in summer and the interface in the Alboran basin at the eastern approach of the Strait deepens.

While the annual cycle of g' forces a phase-locked cycle of the inflowing and outflowing velocities (see Table 3), the deepening of the interface favours the increase of Q_1 and the decrease of $|Q_2|$, and produces a clear annual cycle of Q_{0a} in the manner that the authors' observations indicate. It is worth emphasising that the influence of the interface in the Alboran reservoir only affects the exchange if it is submaximal.

Semiannual signals are more controversial due to the absence of an "a priori" clear driving force. In Section 3 wind stress has been put forward as a candidate, since it has quite a noticeable semiannual cycle that follows the clear cycle of the atmospheric pressure difference. Note that the across-strait sea-level difference in Table 3, $\Delta\xi_T$, behaves like wind stress, suggesting a close cause–effect relationship. The presence of a prevailing semiannual signal in all these variables, at least during CANIGO, allows one to discard an eventual data artifact.

Some of the results shown in Table 3 are worth a special mention: First, the semiannual cycle has no signature in $\Delta\rho$, indicating that it takes place under constant g'; second, semiannual periodicity is absent in Q_1 and only affects Q_2 and η_{2C}; third, inflowing velocity U_1 is above the significance level despite the fact that this is not the case for Q_1, and its phase lies in the error interval of $\Delta\xi_T$, as geostrophy predicts; lastly, and as a consequence of the second point, the net barotropic semiannual signal is introduced via Q_2 and the interface oscillation.

Now, one speculates with a possible mechanism that allows wind stress to drive this cycle. The question then arises as how it would induce a semiannual cycle in the outflow but not in the inflow, which is under the direct influence of wind dragging. As mentioned above, U_1 responds to wind stress showing a semiannual cycle that is not present in Q_1. The semiannual signal of Q_1 has to be lost due to the oscillation of the interface, which is at its highest when U_1 is at its maximum. A possibility is that the signal is forced via interface motions in the Alboran Sea Basin under submaximal exchange again: if it moves upward forced by a positive wind stress (westerly) then the inflowing cross-area is reduced, all of which compensates the greater inflowing speed to produce a negligible signal in Q_1. According to the model of Section 4, the interface rising and the control at CS would imply an increase of the outflow, in the manner indicated in Fig. 7B. The phases of the interface oscillations, wind stress and outflow support this reasoning.

It is easy to show that a wind of stress τ blowing over a two-layer rectangular basin of length L rises the interface in the upwind direction by

$$\Delta\eta_2 = \frac{\tau L}{\rho_2 g' H_1}, \tag{14}$$

where H_1 is the thickness of the upper layer. If this model is applied to an idealized Alboran Sea using the values in Table 3, L must be of the order of 3000 km to obtain a $\Delta\eta_2$ of 8 m. It is well above any reasonable estimate of the length of the Alboran Basin. The mechanism acts in the right direction but the gain is much less than necessary.

Given that the Alboran Basin is not a closed and motionless two-layer rectangular basin, the aforesaid model above is very rough. A numerical model by Macías (1998) indicates that wind can influence the position and size of the WAG. Some observations in the area also support these predictions (Sarhan et al., 2000) in the sense that the gyre would tend to grow and to approach the entrance of the Strait under an easterly wind; the opposite occurring with westerlies. Therefore, the response of the interface to wind force could be enhanced due to the advection of the gyre, and its vertical displacement at the eastern end of the Strait be brought closer to the reported value of 8 m. This needs further verification.

The combination of the annual and semiannual cycles of the interface results in a shallower interface during the first months of the year and a deeper one in late autumn (see Fig. 3). The raising of the interface is faster than its subsequent

drop, which could be related to the rapid filling of the Mediterranean reservoir due to the production of deep water during winter and the subsequent draining of this water through the Strait during the rest of the year. This mechanism was already put forward by Bormans et al. (1986) to explain the seasonal cycle of the interface that they indirectly detected from sea level data.

6. Conclusions

Flows computed from the current-meter time series taken during CANIGO at the eastern end of the Strait of Gibraltar show distinguishable annual and semiannual cycles. They are not coupled in the sense that the inflow only exhibits annual cycle while both annual and semiannual signals are present in the outflow and in the depth of the interface. The semiannual signal is twice as important than the annual one in these last two variables.

It has been shown that a two-layer model with a unique control in the sill section provides a consistent scenario to explain the observations reported here. The absence of the control at the narrowest section implies submaximal exchange, which is further confirmed by the very low values of the composite Froude number estimated at the eastern section (it is worth mentioning that it can eventually reach critical values if meteorologically-induced subinertial and tidal variability are taken into account, as shown in García Lafuente et al. 2000).

The net barotropic flow has a clear annual cycle and a smaller semiannual one that would force sea-level signals in the Mediterranean to appear. Regarding the annual cycle, the mass balance of Eq. (9), which includes the climatological $(E-P)$ term and removes the steric effect on the sea level, confirms the necessity of a net barotropic signal like the one presented here for the sake of validity. A similar conclusion was mentioned by Larnicol et al. (1995) from the analysis of altimetry data. Its origin would be the seasonal signal in the density difference produced by the seasonal warming of the Atlantic waters. The outflow is much less sensitive to this signal. The explanation put forward here is that the exchange is submaximal (very low composite Froude number at the eastern section, see Fig. 8) and that the position of the interface in the Mediterranean reservoir affects the exchange. The increased density contrast during summer develops larger and deeper WAGs that, in turn, sinks the interface in the Strait and reduces the outflow via the control at CS. The inflow takes advantage of two independent facts whose ultimate cause resides in the g' variations: an increased inflowing velocity driven by the enhanced density contrast during summer and a greater inflowing section due to the sinking of the interface. These two facts act in opposite directions on the outflow, reducing in this manner the annual signal of Q_2.

The driving force for the semiannual cycle is not so evident. Wind stress and atmospheric pressure differences show a predominant semiannual cycle, at least during CANIGO, and hence these meteorological agents might be driving forces. The way in which they would produce a more intense cycle in the outflow than in the inflow needs further investigation. At first, Q_1 must be sensitive to direct wind dragging and, in fact, a semiannual signal in the inflowing velocity whose phase agrees with the phase of wind speed has been found. However, the semiannual signal is absent in the inflow. Therefore, the phase of the interface semiannual oscillation must be opposite to that of U_1 in order to cancel the signal in Q_1 and, in fact, it is. Physically, this can happen by means of variations in the depth of the interface in the Alboran basin associated with wind-driven variations of the position and size of the WAG if the exchange is submaximal. Westerly (easterly) winds should induce a raising (sinking) of the interface allowing an increased (diminished) outflow via the CS control. The existence of this control couples the signals of Q_2 and η_{2C} to each other in the manner indicated by the authors' observations (see Table 3). On the other hand, the absence of the TN control allows the cycles of Q_1 and Q_2 to be uncoupled in the sense that Q_1 can change independently of Q_2 and η_2 as Fig. 7B indicates.

The mass balance of Eq. (9) applied to the semiannual cycle does not provide satisfactory results. The poor determination of the semiannual signals in the Mediterranean sea level and in

$(E-P)$ could explain this, although the climatic interannual variability (the data set used to determine each term of Eq. (9) are not simultaneous) may be the cause of the mismatch. In short, the subject requires further research.

Acknowledgements

This work was supported by the European Commission through CANIGO project (MAS3-PL95-0443). Partial support by the Spanish National Program of Marine Science and Technology (MAR95-1950-C02-01) is also acknowledged. The central mooring measurements during the Pilot Phase were supported by the US Office of Naval Research contract N00014-94-1-0347 and by grant OCE-93-13654 from the US National Science Foundation and were taken by Julio Candela in collaboration with Richard Limeburner from Woods Hole Oceanographic Institution and Juan Rico from Instituto Hidrográfico de la Marina, Cadiz, Spain, on board the research vessel Tofiño from this institution. The authors are grateful to them for providing us with these data. Thanks are also due to the captain and crew of the *R/V's Odón de Buen* from IEO and *Poseidon* from Institut für Meereskunde, Germany, for their help in the deployment and recovery of the mooring lines, and to María Jesús García who supplied the sea-level data from the data base of IEO. Comments by an anonymous reviewer have been of great interest to write the final version of the manuscript.

References

Ayoub, N., Le Traon, P.Y., De Mey, P., 1998. A description of the Mediterranean surface variable circulation from combined ERS-1 and TOPEX/POSEIDON altimetric data. Journal of Marine Systems 18, 3–40.

Bascheck, B., Send, U., García Lafuente, J., Candela, J., 2001. Transport estimates in the Strait of Gibraltar with a tidal inverse model. Journal of Geophysical Research 106 (C12), 31,033–31,044.

Bormans, M., Garrett, C., 1989. The effects of non-rectangular cross-section, friction and barotropic fluctuations on the exchange through the Strait of Gibraltar. Journal of Physical Oceanography 19, 1543–1557.

Bormans, M., Garrett, C., Thompson, K.R., 1986. Seasonal variability of the surface inflow through the Strait of Gibraltar. Oceanolog Acta 9, 403–414.

Bryden, H.L., Kinder, T.H., 1991. Steady two-layer exchange through the Strait of Gibraltar. Deep Sea Research 38 (S1), S445–S463.

Bryden, H.L., Candela, J., Kinder, T.H., 1994. Exchange through the Strait of Gibraltar. Progress in Oceanography 33, 201–248.

Candela, J., Winant, C.D., Bryden, H.L., 1989. Meteorologically forced subinertial flows through the Strait of Gibraltar. Journal of Geophysical Research 94, 12,667–12,674.

Candela, J., Winant, C.D., Ruiz, A., 1990. Tides in the Strait of Gibraltar. Journal of Geophysical Research 95, 7313–7335.

Carter, D.B., 1956. The water balance of the Mediterranean and Black Seas. Publ. Climatol. 9, 127–174.

Csanady, G.T., 1979. The birth and death of a warm core ring. Journal of Geophysical Research 84, 777–780.

Farmer, D.M., Armi, L., 1986. Maximal two-layer exchange over a sill and through the combination of a sill and contraction with barotropic flow. Journal of Fluid Mechanics 164, 53–76.

García Lafuente, J., Vargas, J.M., Cano, N., Sarhan, T., Plaza, F., Vargas, M., 1998. Observaciones de corriente en la estación N en el Estrecho de Gibraltar desde Octubre de 1995 a Mayo de 1996. Inf. Téc. Inst. Esp. Oceanogr. 171, 59pp.

García Lafuente, J., Vargas, J.M., Candela, J., Bascheck, B., Plaza, F., Sarhan, T., 2000. The tide at the eastern section of the Strait of Gibraltar. Journal of Geophysical Research 105 (C6), 14,197–14,213.

Garrett, C., 1996. The role of the Strait of Gibraltar in the evolution of Mediterranean water properties and circulation. In: Brain, F. (Ed.), Dynamics of the Mediterranean Straits and Channels, CIESM Science Series 2, Monaco.

Gleizon, P., 1994. Etude experimental de la formation et de la estabilite de tourbillons anticycloniques engendrés par un courant barocline issu d'un détroit. Application à la mer d'Alboran. These de Doctorat de l'Université Joseph Fourier, Grenoble-I, 240pp.

Heburn, G.W., La Violette, P.E., 1990. Variations in the structure of the anticyclonic gyres found in the Alboran Sea. Journal of the Geophysical Research 95, 1599–1613.

Helfrich, K.R., 1995. Time-dependent two-layer hydraulic exchange flows. Journal of the Physical Oceanography 25, 359–373.

Lanoix, F., 1974. Project Alboran, Etude hydrologique et dynamique de la Mer d'Alboran. Technical Report 66, NATO, Brussels, 39pp. plus 32 figs.

Larnicol, G., Le Traon, P.Y., Ayoub, N., De Mey, P., 1995. Mean sea level and surface circulation variability of the Mediterranean Sea from 2 years of TOPEX/POSEIDON altimetry. Journal of the Geophysical Research 100 (C12), 25,163–25,177.

Macías, J., 1998. Simulación numérica en oceanografía. Estudio y desarrollo de un modelo de aguas poco profundas y de un

modelo híbrido de océano-atmósfera. Aplicaciones. Tesis de doctorado de la Universidad de Málaga, 308pp.

MEDATLAS Consortium, 1997. Mediterranean Hydrological Atlas. IFREMER/DITI/IDT, Brest, France.

Patullo, J., Munk, W., Revelle, R., Strong, E., 1955. The seasonal oscillation of sea level. Journal of Marine Research 14, 88–113.

Pinardi, N., Baretta, J.W., Bianchi, M., Crepon, M., Crise, A., Rassoulzadegan, F., Thingstad, F., Zavatarelli, M., 1997. Coupled physical and biological models. In: Lipiatou, E. (Ed.), Interdisciplinary Research in the Mediterranean Sea: A Synthesis of Scientific Results from the Mediterranean Targeted Project (MTP) Phase I, 1993–96. Brussels, pp. 316–342.

Plaza, F., Vargas, M., García Lafuente, J., Vargas, J.M., Sarhan, T., 1999. Is the Alboran passage a good checking point for the Alboran Sea circulation? In Abstracts of the 4th MTP (MATER) Workshop, Perpignan, France, 94.

Sarhan, T., García Lafuente, J., Vargas, M., Vargas, J.M., Plaza, F., 2000. Upwelling mechanisms in the Northwestern Alboran Sea. Journal of Marine Systems 23, 317–331.

Tsimplis, M.N., Woodworth, P.L., 1994. The global distribution of the seasonal sea level cycle calculated from coastal tide gauge data. Journal of Geophysical Research 99 (C8), 16,031–16,039.

Wallen, C.C., 1970. Introduction, climates of northern and western Europe. In: Wallen, C.C. (Ed.), World Survey of Climatology, Vol. 5. Elsevier, New York.

Watson, G., Robinson, I.S., 1990. A study of internal wave propagation in the Strait of Gibraltar using shore-based marine radar images. Journal of Physical Oceanography 20, 374–395.